In situ growth of graphene on hexagonal boron nitride for electronic transport applications

Arjmandi-Tash, Hadi

DOI
10.1039/c9tc04779d

Publication date
2020

Document Version
Final published version

Published in
Journal of Materials Chemistry C

Journal of Materials Chemistry C

ROYAL SOCIETY OF CHEMISTRY

REVIEW

View Article Online
View Journal | View Issue

Cite this: J. Mater. Chem. C, 2020, 8, 380

In situ growth of graphene on hexagonal boron nitride for electronic transport applications

Hadi Arjmandi-Tash

Received 29th August 2019,
Accepted 20th November 2019

DOI: 10.1039/c9tc04779d

rsc.li/materials-c

Transferring graphene flakes onto hexagonal boron nitride (h-BN) has become a common approach for fabricating graphene/h-BN heterostructures. Controlling the alignment between graphene and h-BN lattices is difficult to achieve and the h-BN/graphene interface is prone to contamination in this complicated process. Direct synthesis of graphene on h-BN is a rapidly growing alternative. *In situ* grown graphene is individually tailored to conform to the specific h-BN flake, hence the limitations of the conventional transfer-based fabrication approach are overcome. Developed processes promise improved scalablity of the device fabrication, eventually suitable for industrial applications. The developments in the field, from inception to current status is the focus of this review. How the field is progressing to overcome existing challenges is discussed together with its future prospects.

1 Introduction

Electronic mobility in supported graphene is limited by the roughness and charged impurities on the surface of the substrate.[1–3] Inserting a thick ($\gtrsim$10 nm) buffer layer of hexagonal boron nitride – with an atomically flat and neutral surface – in between the graphene and the supporting substrate helps to overcome those limitations. A heterostructure of graphene on multilayer h-BN flakes was first successfully realized and studied by Dean *et al.*;[4] their device exhibited charge carrier mobilities as high as 140 000 $cm^2\ V^{-1}\ s^{-1}$ which was unapproachable on supported devices at that time. Work from the same group[5] also confirmed the advantages of h-BN as a "mattress" for CVD graphene. Recently by sandwiching graphene between two h-BN layers, long mean free paths (comparable to the device size) and ballistic transport was reported even at room temperature.[6,7] Its dielectric nature and lattice parameter – which is close to that of graphene – are the other remarkable properties of h-BN as a mattress for graphene.

In all these reports, high quality chemically grown[8,9] (*via* chemical vapor deposition (CVD) process) or exfoliated graphene is first isolated on an intermediate substrate and then transferred onto the h-BN flakes. The process has disadvantages: (*i*) contamination of the graphene/h-BN interface by polymeric materials[10,11] (used to assist the transfer) and/or air or water trapping[5] is highly possible. (*ii*) Graphene can be damaged or wrinkled and (*iii*) the process does not provide any control over the relative orientation of graphene and h-BN: the random orientation of the lattices may lead to non-reproducible electronic transport properties. (*iv*) Macroscopic alignment of microscale graphene on h-BN flakes is another issue which is time-consuming and troublesome in practice. Techniques which are transfer-free, involving direct growth of graphene on h-BN offer a solution to overcome the above limitations. Particularly, in such techniques the graphene/h-BN interface is realized *in situ* and thus no external contaminant can be trapped in between.

In this review, the progress of techniques to grow graphene on thick h-BN flakes is outlined. Standard CVD of graphene benefits from the presence of a catalyst (*e.g.*, copper) as a growth promoter; the absence of such a catalyst hinders direct growth of graphene on h-BN. Different approaches to tackling this limitation are discussed and different aspects of *in situ* growth methods are reviewed here. Note, there are some methods developed for growing both graphene and mono- (few-) layered h-BN together to form thin ($\lesssim$10 nm) graphene/h-BN stacks or patchworks;[12–18] Interestingly, the growth of the first sample of this type was reported even before the first isolation of graphene by exfoliation.[19] The thickness of h-BN layers achieved in such approaches, is however, not enough to smooth the roughness of the underlying substrates and diminish the effect of the random potentials resting on the wafer; such approaches are out of the scope of this review.

2 Growth yield

Decomposition of carbon-rich precursor molecules (*e.g.*, methane) in the presence of a catalyst is the central step in conventional CVD of graphene. The elevated temperature of the growth chamber provides enough energy for the resultant carbon

Kavli Institute of Nanoscience, Delft University of Technology, Lorentzweg 1, 2628 CJ Delft, The Netherlands. E-mail: h.arjmanditash@tudelft.nl

atoms to be mobilized, reach and bind to other carbon atoms and eventually form a graphene layer. Indeed, the presence of the catalyst plays an essential role in accelerating the growth: the absence of catalyst is a major limitation for the growth of graphene on arbitrary (*i.e.*, non-catalyst) substrates such as on h-BN.

The first paper about directly growth CVD graphene on h-BN was submitted for publication just four months after the first realization of graphene/h-BN stacking.[4] The rapid progress implies the importance of the *in situ* growth approaches in the first place. Published by Ding *et al.*,[20] this paper confirmed the possibility of chemically growing a few-layer graphene on h-BN powders. The importance of the catalyst was, however, overlooked as no remarkable measure was considered to compensate its absence. The size of the graphene domains remain unclear. Fig. 1a and b shows some of the reported results. Recently and as the field started to develop, a few approaches have been introduced to overcome the absence of the catalyst.

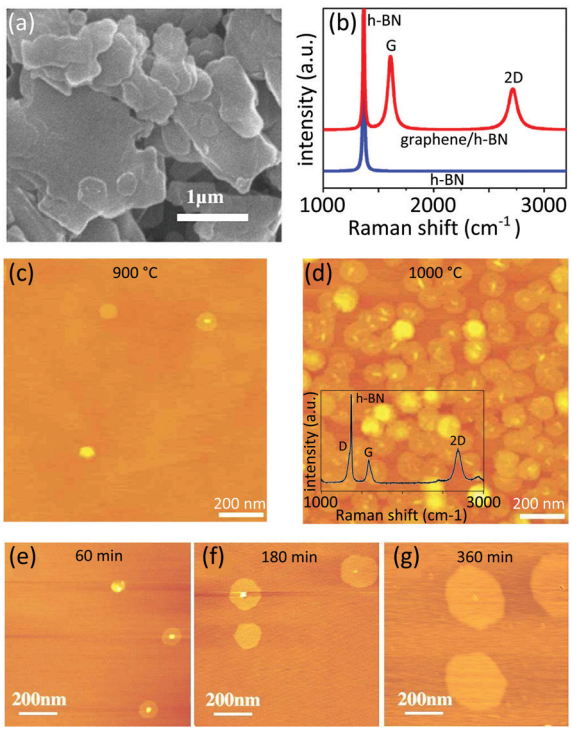

Fig. 1 Early reports on the direct growth of graphene on thick h-BN flakes (a) and (b) results of Ding *et al.*: graphene was grown on h-BN powders through a CVD process. The Raman spectra on (b) are taken from bare h-BN powder and after the growth. Reprinted from ref. 20, Copyright (2011), with permission from Elsevier. (c and d) Results of Son *et al.*: the effect of the growth temperature on the density of the obtained flakes was reported as AFM mappings in this work. The density raised a lot as the temperature increased from 900 °C to 1000 °C. This growth lasts for 2 hours. The inset in (d) shows an example of the Raman spectrum reported on this sample. Adapted from ref. 21 with permission of The Royal Society of Chemistry. (e–g) Results of Tang *et al.*: AFM measurements shown in these figures were performed on the samples with 1, 3 and 6 hours of growth. Reprinted from ref. 22, © 2012, with permission from Elsevier.

2.1 Elongated growth

Elongating the growth course is a direct () approach to compensate for the absence of catalyst. Son *et al.*[21] mechanically exfoliated h-BN flakes on a silicon wafer and grew graphene in an atmospheric pressure CVD chamber. Different growth temperatures ranging between 900 °C to 1000 °C with a similar growth duration of 2 hours were tested. Domains of ~100 nm in diameter achieved. They reported a direct trend of increasing the density of the graphene pads upon increasing the growth temperature (Fig. 1c and d). The grown graphene flakes were of rounded shape with thicknesses of the order of 0.5 nm. AFM, Raman and XPS analysis have been performed to confirm the growth and characterize the graphene.

This approach was followed later by Tang *et al.*[22] Like Son's experiment, graphene was grown on hexagonal boron nitride flakes exfoliated on silicon wafer, albeit through a low pressure CVD process. They noticed that screw dislocations on the flakes are favorable nucleation sites. The slow growth rate due to the absence of catalyst was evident in the results reported; a growth duration of 6 hours only led to the formation of graphene grains of a maximum 270 nm in diameter (Fig. 1e–g). The graphene domains were mostly single layer.

Elongating the growth – although simple – has certain drawbacks: the reported graphene domains – even after several hours of growth – barely reached a few hundred nanometers and are incompatible with typical device fabrication processes. The long operation time and high energy consumption are unfavorable for industrial application.

2.2 Optimized growth parameters

Fine-tuning the growth parameters is a wiser approach to improve the yield. Mishra *et al.*[23] showed that in a typical CVD process, increasing the partial pressure of hydrogen and elevating the growth temperature can achieve an improved growth rate of up to 100 nm min^{-1} (to be compared with 5 nm min^{-1} with standard CVD growth parameters[24]) (Fig. 2a). They systematically investigated the effect of the partial pressure of hydrogen on the crystallinity of the grown graphene domains: low partial pressure of hydrogen (H_2 to CH_4 ratio of 1 : 1) mainly achieved circular poly-crystalline grains. Increasing the partial pressure of hydrogen (H_2 to CH_4 ratio of 30 : 1), however, led to the formation of van der Waals epitaxy with aligned hexagonal grains. Indeed, reducing the density of nucleation centers *via* hydrogen etching plays a vital role in the reported results.

2.3 Plasma-enhanced chemical vapor deposition

Inspired by earlier works on the growth of graphene on non-catalyst substrates,[25,26] Yang *et al.* employed the remote plasma-enhanced chemical vapor deposition (RPE-CVD) technique to grow graphene on exfoliated h-BN flakes.[27] Here, a remote plasma source decomposes methane molecules into various reactive radicals prior to reaching the substrate; hence the catalyst can be omitted. The approach provides enough control over the number of layers and uniformity of graphene.

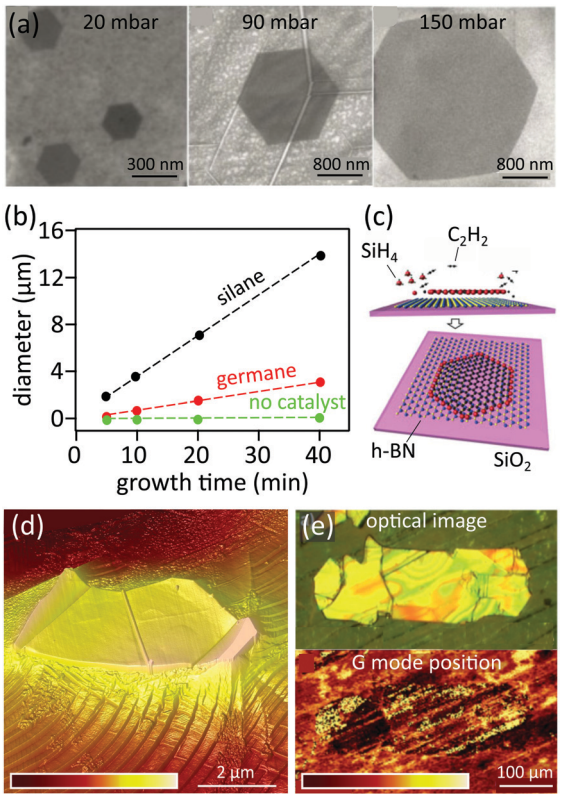

Fig. 2 Various approaches to improve the growth rate (a) effect of increasing the growth pressure on the grain size: SEM images showing graphene grains synthesized on h-BN flakes at 1150 °C under various chamber pressures. Reprinted from ref. 23, © 2016, with permission from Elsevier. (b and c) Gaseous phase catalyst to improve the growth rate: (b) comparison of the experimentally measured grain size of graphene flakes grown at 1280 °C with and without gaseous catalysts. (c) Schematic illustration showing the mechanism of growing monolayer graphene onto h-BN: silicon atoms (shown as red color spheres) achieved from the decomposition of SiH_4 bound to the edge of the graphene and boosting the growth. Adapted from ref. 24. (d and e) Proximity driven over growth of graphene onto h-BN flakes pre-exfoliated on the copper foil: (d) AFM mapping showing an h-BN flake (covered with graphene) on the copper foil at the end of the growth course. The color code shows the height, ranging between 0 nm and 500 nm. (e) Optical image (top) and Raman G mode position mapping (bottom) of a millimeter scale h-BN flake on the copper foil, fully covered by graphene. The color code shows the Raman frequency ranging between 1584 cm^{-1} and 1600 cm^{-1}. Adapted from ref. 28.

In principal, the size of the graphene is only limited by the size of underlying h-BN flakes. Growth temperature controls both the epitaxy and the rate of the growth: even-though increasing the growth temperature improves the growth rate, the population of nucleation centers also increases at the same time which may lead to three-dimensional – instead of layer-by-layer – growth and suppress the epitaxy. The growth temperature of ~500 °C was the best compromise between epitaxy and the growth rate. In this condition, several growth periods, each of two to three hours are still required to obtain the desired graphene sizes.

2.4 Gaseous catalyst

While the presence of the h-BN as a background substrate does not leave any room for a solid catalyst, Tang *et al.*[24] used gaseous silane (SiH_4) and germane (GeH_4) catalysts to boost the growth. At a temperature of 1280 °C, the growth rate reached 50 nm min^{-1} and 400 nm min^{-1}, respectively in the presence of germane and silane: the yield was improved significantly compared to the recorded 5 nm min^{-1} in the absence of any catalyst. Elevating the growth temperature up to 1350 °C further accelerated the growth rate reaching ~1 μm min^{-1} (Fig. 2b). Importantly, Auger electron spectroscopy of the domains did not show any trace of silicon or germanium in the grown graphene crystal. Apparently, those atoms only stick to the edge of the graphene domains and lower the reaction barrier for carbon precursors to form the honeycomb lattice during growth (Fig. 2c). AFM analyses confirmed that more than 93% of the graphene domains are well oriented with respect to the background lattice of h-BN.

2.5 Proximity-driven overgrowth

A new approach in the growth of graphene on non-catalyst materials such as h-BN was introduced recently.[28] Unlike previous approaches, the growth is performed on h-BN flakes which are pre-exfoliated on copper foil (Fig. 2d). Hence, the carbon-rich precursors still have access to the catalyst, albeit indirectly. The growth rate of graphene on h-BN was improved dramatically: a full coverage of graphene on millimeter sized h-BN flake is achievable in the same rate of graphene on the surrounding copper foil (Fig. 2e). The obtained devices exhibited charge carrier mobilities of 20 000 cm^2 V^{-1} s^{-1} and neutral graphene–h-BN interfaces.

3 Growth mechanism

In fabricating heterostructures by depositing a material on a substrate at least two mechanisms are feasible: in materials with terminating layers full of dangling bonds, atoms in one material can establish covalent bonds only to the atoms of a similar lattice; indeed, the covalent bonds are sensitive to the length and angle between the atoms. This is an important hindrance in epitaxial growth between materials with different lattice parameters. Fig. 3a schematically illustrates this mechanism. The situation is different between two materials with perfect terminating surfaces and no dangling bonds (Fig. 3b). Here, the absence of the dangling bonds can lead to the formation of sharp interfaces with a small amount of defects. This growth mechanism is referred to as van der Waals epitaxy and can be realized even in the presence of large lattice mismatches.[29,30] As graphene and h-BN are both free from dangling bonds, van der Waals epitaxy is normally the governing growth mechanism.

Garcia *et al.*[31] first reported van der Waals epitaxy in *in situ* growth of graphene on h-BN. Unlike previous experiments, graphene was grown by molecular beam epitaxy (MBE) using solid carbon sources. Combined Raman and AFM analysis revealed that the growth is independent of the flux of carbon atoms; instead, carbon atoms deposed on the surface, migrate freely and accumulate in selective spots on the h-BN surface (Fig. 3b and c).

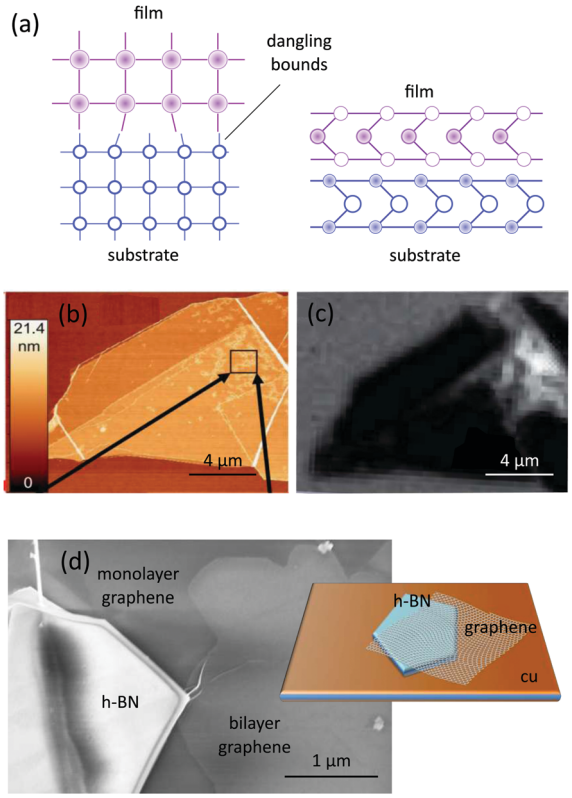

Fig. 3 Known mechanisms governing the growth of graphene on h-BN flakes. (a) Comparison of the epitaxial growth between materials with (left) and without (right) dangling bonds, the latter has been dubbed van der Waals epitaxy; in both cases the atoms, corresponding to the substrate and to the deposited film are shown in blue and pink, respectively. (b) AFM and (c) Raman (intensity of 2D peak of graphene) mapping of a h-BN flake with deposited graphene *via* molecular beam epitaxy; the mappings show that carbon atoms are freely migrated and accumulated in some preferential spots on the surface of h-BN. Reprinted from ref. 31, © 2012, with permission from Elsevier. (d) Schematic representation of the mechanism (inset) and SEM image of graphene (both mono- and bi-layer) nucleated on the copper foil and extended over the h-BN flake *via* proximity driven growth. Adapted from ref. 28.

This observation indicated that the carbon atoms are of high mobility on the neutral h-BN, confirming that van der Waals epitaxy is achieved. Recently, van der Waals epitaxy was reported in CVD growth of graphene on h-BN also.[23] The lack of any covalent bond results in weak interfacial interaction between graphene and h-BN.[16]

A separate but complementary growth mechanism involves extending graphene – already nucleated on the copper foil – onto nearby h-BN flakes. This mechanism was first observed in graphene grown on few-layer chemically grown h-BN sheets;[15] our recent work,[28] however, confirmed that the thickness of the h-BN is not any limitation as graphene can overgrow on hundreds-of-nanometers-thick h-BN flakes, mechanically pre-exfoliated on the copper foil. Inset to Fig. 3d explains our hypothesized model for this growth. Precursors are cracked on the copper foil. The achieved carbon radicals move randomly in different directions and are energetic enough to continuously jump over the h-BN flake and bond as-growing graphene. The presence of the copper catalyst and high mobility of carbon atoms – as a result of the van der Waals epitaxy – guarantees a high growth rate atop h-BN flakes. The main panel of Fig. 3d shows a SEM image of a h-BN flake covered with graphene.

4 Epitaxial growth

Once two similar patterns of crystalline lattices (*e.g.*, graphene and h-BN lattices) are superimposed with a small displacement or rotation in between, a secondary pattern known as moiré generates.[32,33] The moiré superlattice potential affects the propagation of charge carriers in graphene by inducing new Dirac points, known as Satellite Dirac Points (SDPs) in the band structure of graphene. The energy of SDPs (E_{SDP}) depends on the wave vector of the superlattice (λ_{SL}) which itself is a function of the misorientation angle (Φ) between the lattices:[34]

$$E_{SDP} = \pm\frac{\hbar v_f\left|\vec{G}\right|}{2} = \pm\frac{2\pi\hbar v_F}{\sqrt{3}\lambda_{SL}},$$

where

$$\lambda_{SL} = \frac{(1+\delta)a}{\sqrt{2(1+\delta)(1-\cos\Phi)+\delta^2}}$$

In this relation, $\vec{G}$ represents the reciprocal superlattice vector and $v_F \approx 10^6$ m s^{-1} is the Fermi velocity of quasiparticles in graphene. Additionally, a = 2.46 Å and δ = 1.8% are the lattice parameter of graphene and the mismatch between graphene and h-BN lattices, respectively.

Controlling and minimizing the misorientation angle in graphene/h-BN heterostructures is of great importance to lower structural uncertainties. Indeed the traditional method of transferring exfoliated graphene on h-BN leads to a random orientation of the lattices. Although recent progress in the field has revealed that post-treatment of the samples at elevated temperatures can drive graphene to rotate and follow h-BN lattices,[35,36] such approaches are more efficient in sub-micrometer flakes. *In situ* grown graphene on h-BN, however, has proven capabilities for controlling Φ in much larger samples.

Yang *et al.* utilized the plasma-enhanced CVD technique to grow graphene on mechanically exfoliated h-BN flakes.[27] Large area, epitaxial and single crystal graphene domains directly grown on the h-BN flakes were obtained. Breaking down the methane molecules with a remote plasma source eliminated the need for a catalyst and enhanced the growth rate and the domain size. The cleanness of the flakes was sufficient that they managed to observe the moiré pattern associated with the superposition of graphene and h-BN crystals by AFM analysis (Fig. 4a and b). This analysis showed that the graphene lattice follows the orientation of the underlying h-BN. The size of the graphene was limited by the size of the h-BN flake, large enough to fabricate devices for transport experiments. The signature of the superposition of the lattices as extra Dirac points in the resistivity and quantum Hall effect measurements was revealed at low temperature (Fig. 4c and d).

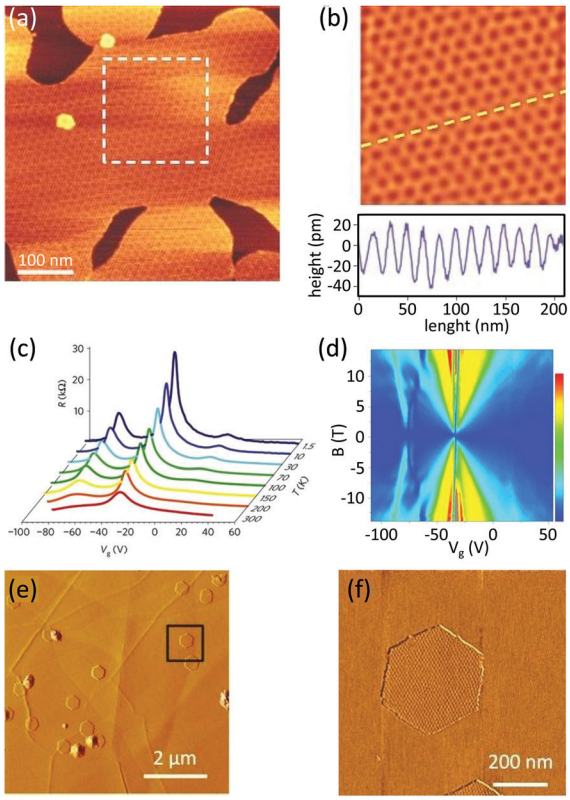

Fig. 4 Crystalline biased growth of graphene on h-BN (a) moiré pattern due to the superposition of the graphene and h-BN lattices, (b) filtered inverse fast Fourier transform of the pattern is visible in the dashed square in a, height profile along the dashed line is shown in the lower part. The periodicity of the oscillations can be used to calculate the rotation angle between the lattices. Reprinted by permission from Macmillan Publishers Ltd: Nature Materials,[27] © 2013. (c) Gate dependence of the resistivity measured at different temperatures: satellite peaks shown at the left and right side of the Dirac point are due to the formation of the superlattice. (d) This effect can also be seen as the pattern at the left side of the fan diagram of R_{xy} in the quantum hall measurement. Reprinted by permission from Macmillan Publishers Ltd: Nature Materials,[27] © 2013. (e) Topography of the small graphene flakes and (f) moiré pattern associated with graphene/h-BN superposition. Reprinted with adaptations from ref. 37. The mappings shown in a, b, e and f are obtained with atomic force microscopy.

Note that a similar alignment was reported later by Tang *et al.*[24,37] (Fig. 4e and f) and Mishra *et al.*[23]

5 Discussion

Table 1 summarizes the important reports of *in situ* grown graphene on thick (≫monolayer) h-BN flakes in a chronological order. Chemical vapor deposition (including its derivatives) using methane precursor has been the most frequently employed method. Such reports demonstrated the growth in a wide temperature range.

The size of the resultant graphene samples and growth rate have been improved gradually over the last years. Similar improvements in controlling the thickness (number of layers) of graphene is also detectable. While the orientation of graphene in early reports was unclear, recent works have reported a trend in graphene/h-BN lattice alignment. The best mobility reported for *in situ* grown samples is still much inferior than that achieved in transfer-fabricated samples, even with CVD graphene[5] which highlights the affect of crystalline defects. Indeed, the techniques employed to compensate for the lack of catalyst – even-though successful to preserve the growth rate – have still failed to yield crystalline qualities comparable to that of graphene grown on a catalyst.

6 Conclusion and perspective

The outstanding electrical properties of graphene are effectively preserved from substrate-related perturbations by thick (few tens of nanometers) h-BN buffer layers. The conventional fabrication approach – involving graphene transferring on to h-BN flakes – is prone to mechanically altering (*e.g.*, tearing, wrinkling, stretching) the graphene. The interface contaminations by alien materials and/or air trapping are common limitations.[39] The process is time-consuming and the success rate heavily depends on the expertise of the user. *In situ* growth of graphene on h-BN provides a route for achieving clean interfaces.

Chemical vapor deposition (CVD) has been qualified as an effective *in situ* growth approach. The lack of a catalyst

Table 1 Summary of the reports of *in situ* grown graphene on thick h-BN flakes, in chronological order

Report	Process	Precursor	Temperature (°C)	Duration	Size	Thickness	Orientated[a]	Mobility
Ding[20]	CVD	CH_4 (50–90 sccm)	1000	3–8 min	Not reported	>6 L	Unclear	Not reported
Son[21]	CVD	CH_4 (30–50 sccm)	900–1000	2 h	100 nm	≈0.5 nm	Unclear	Not reported
Tang[22]	CVD	CH_4 (5 sccm)	1200	1–6 h	<270 nm	ML	unclear	Not reported
Garcia[31]	MBE	Solid carbon	600–930	40.6 min	nm-scale	ML	Unclear	Not reported
Yang[27]	PECVD	CH_4[b]	≈500	≫3 h	μm-scale	ML & BL	Yes	~5000 $cm^2 V^{-1} s^{-1}$ (at 1.5 K)
Tang[37]	CVD	CH_4 (5 sccm)	1200	1–5 h	μm-scale	ML & BL	Yes	20 000 $cm^2 V^{-1} s^{-1}$ (at 300 K)
Tang[24]	CVD	C_2H_2[b]	1280–1350	5–40 min	μm-scale	ML	Yes	20 000 $cm^2 V^{-1} s^{-1}$ (at 300 K)
Mishra[23]	Cold-wall CVD	CH_4[b]	1000–1150	30 min	μm-scale	ML	Yes	Not reported
Arjmandi-Tash[28]	CVD	CH_4 (5 sccm)	1050	90 s	mm-scale	ML	Unclear	20 000 $cm^2 V^{-1} s^{-1}$ (at 80 K)
Plaut[38]	MBE	Solid carbon	500–1000	65 min	μm-scale	ML	Unclear	Not reported

ML: monolayer, BL: bilayer. [a] If graphene follows the orientation of underlying h-BN. [b] The flow rate of the precursor was not reported in this work.

material – otherwise existing in conventional CVD of graphene on a metallic foil – is a great hindrance in the development of the process. In-fact early attempts compensated the slow chemical reaction by considerably elongating the growth up to hours and days. The new development in which the catalyst material indirectly promotes the graphene growth on h-BN[28] is a breakthrough as the full coverage of graphene on millimeter scale h-BN flakes can now be achieved at rates identical to those on a catalyst. The electronic transport characteristics of graphene achieved by *in situ* growth approaches are still inferior than the devices achieved in transfer-fabricated methods. In fact, while the charge carrier mobility of *in situ* grown graphene fails to exceed 20 000 $cm^2\ V^{-1}\ s^{-1}$, ballistic transport with tens to hundreds times higher mobilities are now commonly achieved with transfer-fabricated graphene/h-BN heterostructures.[6,7] Indeed, largely found crystalline defects serve as charge carrier scattering centers and strongly suppress the carrier mobility in *in situ* grown graphene. Certain measures, including the optimization of the growth parameters have to be taken to improve the crystalline order of graphene in the future. The electronic band structure of van der Waals heterostructures can be customized by engineering the twist angle between crystals (moiré superlattice potential). In-fact precise control of the twist angle achieves insulating, semi-metallic and superconducting states in such heterostructures.[40,41] Herein, the *in situ* growth approaches offer great potential as the orientation of the growing graphene is governed by the crystalline orientation of the background h-BN. Sandwiching graphene in between two h-BN flakes provides the optimum device quality; as yet *in situ* growth methods have failed to yield such structures. Additionally, direct growth of van der Waals hetero-structures with multiple two-dimensional materials is on the horizon. The choice of CVD for the *in situ* growth of graphene on h-BN is largely motivated by the proven qualification of the method in growing graphene on copper. Unlike on copper, the growth is not self-limited on h-BN and does not guarantee a uniform monolayer film thickness. Although the observation of restricted monolayer growth on an h-BN ridge in MBE[38] is promising, customizing the number of layers is so far out of reach. Besides CVD and MBE, certain efforts have to be made to evaluate the efficiency of other exiting approaches (*e.g.*, bottom-up synthesis using polycyclic aromatic hydrocarbons) or developing novel modalities in *in situ* growing graphene on h-BN in the future.

Conflicts of interest

There are no conflicts to declare.

References

1 E. Hwang, S. Adam and S. Sarma, *Phys. Rev. Lett.*, 2007, **98**, 186806.
2 X. Du, I. Skachko, A. Barker and E. Y. Andrei, *Nat. Nanotechnol.*, 2008, **3**, 491–495.
3 A. S. Mayorov, D. C. Elias, I. S. Mukhin, S. V. Morozov, L. A. Ponomarenko, K. S. Novoselov, A. K. Geim and R. V. Gorbachev, *Nano Lett.*, 2012, **12**, 4629–4634.
4 C. R. Dean, A. F. Young, I. Meric, C. Lee, L. Wang, S. Sorgenfrei, K. Watanabe, T. Taniguchi, P. Kim, K. L. Shepard and J. Hone, *Nat. Nanotechnol.*, 2010, **5**, 722–726.
5 N. Petrone, C. R. Dean, I. Meric, A. M. van der Zande, P. Y. Huang, L. Wang, D. Muller, K. L. Shepard and J. Hone, *Nano Lett.*, 2012, **12**, 2751–2756.
6 A. S. Mayorov, R. V. Gorbachev, S. V. Morozov, L. Britnell, R. Jalil, L. A. Ponomarenko, P. Blake, K. S. Novoselov, K. Watanabe, T. Taniguchi and A. K. Geim, *Nano Lett.*, 2011, **11**, 2396–2399.
7 L. Wang, I. Meric, P. Y. Huang, Q. Gao, Y. Gao, H. Tran, T. Taniguchi, K. Watanabe, L. M. Campos, D. A. Muller, J. Guo, P. Kim, J. Hone, K. L. Shepard and C. R. Dean, *Science*, 2013, **342**, 614–617.
8 Z. Han, A. Kimouche, D. Kalita, A. Allain, H. Arjmandi-Tash, A. Reserbat-Plantey, L. Marty, S. Pairis, V. Reita, N. Bendiab, J. Coraux and V. Bouchiat, *Adv. Funct. Mater.*, 2014, **24**, 964–970.
9 H. Arjmandi-Tash, N. Lebedev, P. van Deursen, J. Aarts and G. F. Schneider, *Carbon*, 2017, **118**, 438–442.
10 L. A. Belyaeva, W. Fu, H. Arjmandi-Tash and G. F. Schneider, *ACS Cent. Sci.*, 2016, **2**, 904–909.
11 L. M. C. Lima, H. Arjmandi-Tash and G. F. Schneider, *ACS Appl. Mater. Interfaces*, 2018, **10**, 11328–11332.
12 M. Wang, S. K. Jang, W.-J. Jang, M. Kim, S.-Y. Park, S.-W. Kim, S.-J. Kahng, J.-Y. Choi, R. S. Ruoff, Y. J. Song and S. Lee, *Adv. Mater.*, 2013, **25**, 2746–2752.
13 S. Roth, F. Matsui, T. Greber and J. Osterwalder, *Nano Lett.*, 2013, **13**, 2668–2675.
14 Z. Liu, L. Song, S. Zhao, J. Huang, L. Ma, J. Zhang, J. Lou and P. M. Ajayan, *Nano Lett.*, 2011, **11**, 2032–2037.
15 S. M. Kim, A. Hsu, P. T. Araujo, Y.-H. Lee, T. Palacios, M. Dresselhaus, J.-C. Idrobo, K. K. Kim and J. Kong, *Nano Lett.*, 2013, **13**, 933–941.
16 S. Entani, M. Takizawa, S. Li, H. Naramoto and S. Sakai, *Appl. Surf. Sci.*, 2019, **475**, 6–11.
17 Q. Wu, J. Lee, J. Sun and Y. J. Song, *Carbon*, 2018, **138**, 76–80.
18 X. Song, T. Gao, Y. Nie, J. Zhuang, J. Sun, D. Ma, J. Shi, Y. Lin, F. Ding, Y. Zhang and Z. Liu, *Nano Lett.*, 2016, **16**, 6109–6116.
19 C. Oshima, A. Itoh, E. Rokuta, T. Tanaka, K. Yamashita and T. Sakurai, *Solid State Commun.*, 2000, **116**, 37–40.
20 X. Ding, G. Ding, X. Xie, F. Huang and M. Jiang, *Carbon*, 2011, **49**, 2522–2525.
21 M. Son, H. Lim, M. Hong and H. C. Choi, *Nanoscale*, 2011, **3**, 3089–3093.
22 L. A. L. Tang, W. C. Lee, H. Shi, E. Y. L. Wong, A. Sadovoy, S. Gorelik, J. Hobley, C. T. Lim and K. P. Loh, *Small*, 2012, **8**, 423–431.
23 N. Mishra, V. Miseikis, D. Convertino, M. Gemmi, V. Piazza and C. Coletti, *Carbon*, 2016, **96**, 497–502.
24 S. Tang, H. Wang, H. S. Wang, Q. Sun, X. Zhang, C. Cong, H. Xie, X. Liu, X. Zhou, F. Huang, X. Chen, T. Yu, F. Ding, X. Xie and M. Jiang, *Nat. Commun.*, 2015, **6**, 6499.

25 L. Zhang, Z. Shi, Y. Wang, R. Yang, D. Shi and G. Zhang, *Nano Res.*, 2011, **4**, 315–321.
26 L. Zhang, Z. Shi, D. Liu, R. Yang, D. Shi and G. Zhang, *Nano Res.*, 2012, **5**, 258–264.
27 W. Yang, G. Chen, Z. Shi, C.-C. Liu, L. Zhang, G. Xie, M. Cheng, D. Wang, R. Yang, D. Shi, K. Watanabe and T. Taniguchi, *Nat. Mater.*, 2013, **12**, 792–797.
28 H. Arjmandi-Tash, D. Kalita, Z. Han, R. Othmen, G. Nayak, C. Berne, J. Landers, K. Watanabe, T. Taniguchi, L. Marty, J. Coraux, N. Bendiab and V. Bouchiat, *J. Phys. Mater.*, 2018, **1**, 015003.
29 K. Ueno, K. Sasaki, N. Takeda, K. Saiki and A. Koma, *Appl. Phys. Lett.*, 1997, **70**, 1104.
30 K. Sasaki, K. Ueno and A. Koma, *Jpn. J. Appl. Phys.*, 1997, **36**, 4061–4064.
31 J. M. Garcia, U. Wurstbauer, A. Levy, L. N. Pfeiffer, A. Pinczuk, A. S. Plaut, L. Wang, C. R. Dean, R. Buizza, A. M. Van Der Zande, J. Hone, K. Watanabe and T. Taniguchi, *Solid State Commun.*, 2012, **152**, 975–978.
32 J. Xue, J. Sanchez-yamagishi, D. Bulmash, P. Jacquod, A. Deshpande, K. Watanabe, T. Taniguchi, P. Jarillo-herrero and B. J. Leroy, *Nat. Mater.*, 2011, **10**, 282–285.
33 R. Decker, Y. Wang, V. W. Brar, W. Regan, H.-Z. Tsai, Q. Wu, W. Gannett, A. Zettl and M. F. Crommie, *Nano Lett.*, 2011, **11**, 2291–2295.
34 M. Yankowitz, J. Xue, D. Cormode, J. D. Sanchez-Yamagishi, K. Watanabe, T. Taniguchi, P. Jarillo-Herrero, P. Jacquod and B. J. LeRoy, *Nat. Phys.*, 2012, **8**, 382–386.
35 D. Wang, G. Chen, C. Li, M. Cheng, W. Yang, S. Wu, G. Xie, J. Zhang, J. Zhao, X. Lu, P. Chen, G. Wang, J. Meng, J. Tang, R. Yang, C. He, D. Liu, D. Shi, K. Watanabe, T. Taniguchi, J. Feng, Y. Zhang and G. Zhang, *Phys. Rev. Lett.*, 2016, **116**, 1–6.
36 C. R. Woods, F. Withers, M. J. Zhu, Y. Cao, G. Yu, A. Kozikov, M. Ben Shalom, S. V. Morozov, M. M. van Wijk, A. Fasolino, M. I. Katsnelson, K. Watanabe, T. Taniguchi, A. K. Geim, A. Mishchenko and K. S. Novoselov, *Nat. Commun.*, 2016, **7**, 10800.
37 S. Tang, H. Wang, Y. Zhang, A. Li, H. Xie, X. Liu, L. Liu, T. Li, F. Huang, X. Xie and M. Jiang, *Sci. Rep.*, 2013, **3**, 2666.
38 A. S. Plaut, U. Wurstbauer, S. Wang, A. L. Levy, L. Fernandes dos Santos, L. Wang, L. N. Pfeiffer, K. Watanabe, T. Taniguchi, C. R. Dean, J. Hone, A. Pinczuk and J. M. Garcia, *Carbon*, 2017, **114**, 579–584.
39 T. Uwanno, Y. Hattori, T. Taniguchi, K. Watanabe and K. Nagashio, *2D Mater.*, 2015, **2**, 041002.
40 Y. Cao, V. Fatemi, S. Fang, K. Watanabe, T. Taniguchi, E. Kaxiras and P. Jarillo-Herrero, *Nature*, 2018, **556**, 43–50.
41 E. Codecido, Q. Wang, R. Koester, S. Che, H. Tian, R. Lv, S. Tran, K. Watanabe, T. Taniguchi, F. Zhang, M. Bockrath and C. N. Lau, *Sci. Adv.*, 2019, **5**, eaaw9770.

